Mon. Not. R. Astron. Soc. **330,** 365–377 (2002)

Source–lens clustering effects on the skewness of the lensing convergence

Takashi Hamana,[1★†] Stéphane T. Colombi,[1,2] Aurélien Thion,[1] Julien E. G. T. Devriendt,[3] Yannick Mellier[1,4] and Francis Bernardeau[5]

[1]*Institut d'Astrophysique de Paris, CNRS, 98bis Boulevard Arago, F75014 Paris, France*
[2]*NIC (Numerical Investigations in Cosmology), CNRS*
[3]*Nuclear & Astrophysics Laboratory, University of Oxford, Keble Road, OX1 3RH*
[4]*Observatoire de Paris, DEMIRM, 61 avenue de l'Observatoire, 75014 Paris, France*
[5]*Service de Physique Théorique, C.E. de Saclay, 91191 Gif sur Yvette Cedex, France*

Accepted 2001 October 18. Received 2001 October 3; in original form 2000 December 13

ABSTRACT

The correlation between source galaxies and lensing potentials causes a systematic effect on measurements of cosmic shear statistics, known as the source–lens clustering (SLC) effect. The SLC effect on the skewness of lensing convergence, S_3, is examined using a non-linear semi-analytic approach and is checked against numerical simulations. The semi-analytic calculations have been performed in a wide variety of generic models for the redshift distribution of source galaxies and power-law models for the bias parameter between the galaxy and dark matter distributions. The semi-analytic predictions are tested successfully against numerical simulations. We find the relative amplitude of the SLC effect on S_3 to be of the order of 5–40 per cent. It depends significantly on the redshift distribution of sources and on the way in which the bias parameter evolves. We discuss possible measurement strategies to minimize the SLC effects.

Key words: gravitational lensing – cosmology: theory – dark matter – large-scale structure of Universe.

1 INTRODUCTION

Recent detections of the cosmic shear signal have opened a new window to probe the distribution of matter in the Universe and its evolution, and to test cosmological models (Van Waerbeke et al. 2000; Wittman et al. 2000; Bacon, Refregier & Ellis 2000; Kaiser, Wilson & Luppino 2000; Maoli et al. 2001). These detections have been obtained from relatively small fields so far, which limits the statistical analysis of the surveys to second-order moments, the variance or two-point correlation function of cosmic shear. The amplitude of second-order statistics reflects that of density fluctuations and roughly scales as $\sigma_\gamma \propto \Omega_{\rm m}^{0.6-0.8}\sigma_8$ at large scales (Bernardeau, Van Waerbeke & Mellier 1997, hereafter BvWM97) and $\sigma_\gamma \propto \Omega_{\rm m}^{0.6-0.8}\sigma_8^{1.2-1.3}$ at small scales (Jain & Seljak 1997; Maoli et al. 2001). On the other hand, the skewness (a third-order statistic) of lensing convergence is known to be sensitive to $\Omega_{\rm m}$, almost independently of σ_8 (BvWM97). Therefore combined analysis of the skewness and the variance will provide precious constraints on values of both $\Omega_{\rm m}$ and σ_8. As a consequence, skewness measurement is one of the main goals of on-going wide field cosmic shear surveys such as the DESCART project.[1]

Cosmic shear statistics have been studied analytically [see Mellier (1999) and Bartelmann & Schneider (2001) for reviews, and references therein] as well as numerically (Jain, Seljak & White 2000; White & Hu 2000). The skewness of lensing convergence was first calculated by BvWM97 based on a quasi-linear perturbation theory approach. It has however, been recognized that this approach is not robust enough to provide accurate predictions for the value of the skewness over the whole available dynamic range. In particular, the following two points have to be addressed and carefully included in the calculations: (i) non-linear growth of the density field – numerical studies show that non-linear growth enhances skewness, especially at angular scales smaller than 1° (Jain et al. 2000; White & Hu 2000; Van Waerbeke et al. 2001b); (ii) source clustering – Bernardeau (1998, hereafter B98) pointed out that correlations between source galaxies and lensing potential reduce skewness amplitude. B98 underlined that this effect is sensitive to the redshift distribution of sources.

The purpose of this paper is to examine the effect of source–lens clustering (SLC) on measurements of the skewness of lensing convergence. Special attention is paid to its dependence on the redshift distribution of sources and on evolution of the bias relation

★ Present address: National Astronomical Observatory of Japan, Mitaka, Tokyo 181-8588, Japan.

[1] For more information about the DESCART project, see http://terapix.iap.fr/Descart/

†E-mail: hamana@yukawa.kyoto-u.ac.jp

between the matter and galaxy distributions. Since the redshift distribution of faint galaxies is uncertain and little is known about the bias, this paper does not aim to make accurate predictions for the amplitude of the SLC effect in real cosmic shear surveys. Our objective is to estimate its magnitude in order to propose strategies that minimize its effects.

We basically follow the perturbation theory approach first developed by B98 but generalize it in two ways: (i) we take into account the effects of non-linear evolution of the density field, adopting the non-linear semi-analytic ansatz developed by Jain & Seljak (1997) and Van Waerbeke et al. (2001b); (ii) we allow a possible redshift dependence of the bias parameter, $b(z) = b_0(1+z)^{\gamma}$, and examine the cases $\gamma = 0$ to 2. Moreover, we consider three cosmological cold dark matter family models (CDM), two flat models with and without a cosmological constant and an open model, and 12 different models for the source distribution which cover a wide range of mean redshift and width for the distribution.

Finally, for the first time the accuracy of semi-analytic predictions for the SLC effects on the skewness is tested against numerical simulations in the standard CDM model.

The outline of this paper is as follows. In Section 2, the physical mechanism of SLC is described. In Section 3, an expression for the skewness of lensing convergence is presented that takes both SLC and non-linear evolution of the density field into account. In Section 4, our models are described. Results of the semi-analytic approach are presented in Section 5. In Section 6, semi-analytic predictions are tested against numerical simulations. We summarize and discuss our conclusions in Section 7. The derivation of the convergence skewness in the presence of the SLC is presented in Appendix A. The *N*-body data sets and the ray-tracing method used for this work are described in Appendix B. In Appendix C, details of the procedure to generate mock galaxy catalogues are presented.

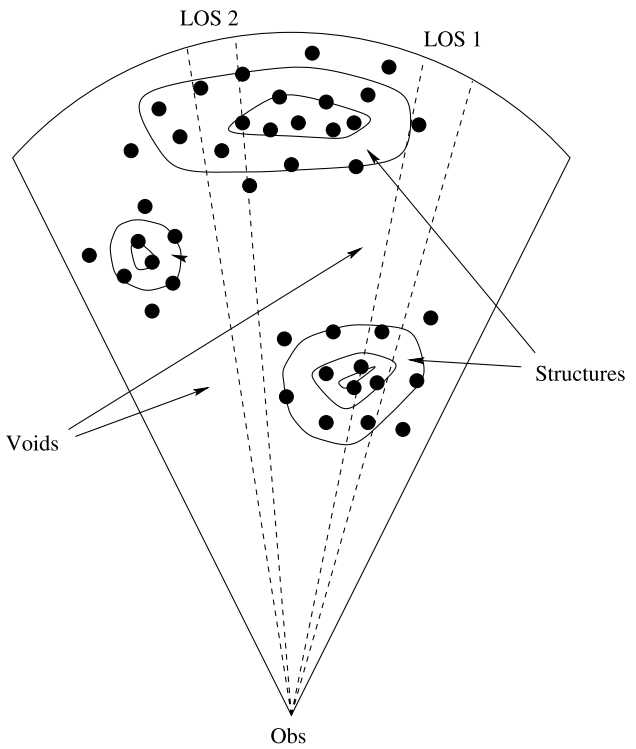

Figure 1. An illustration of the correlation between the gravitational potential (contour lines) and the population of sources (denoted by filled circles).

2 WHAT IS THE SLC EFFECT?

The SLC effect discussed in this paper comes to light because of the conjunction of three circumstances, namely (i) source galaxies are not randomly distributed in the sky but are correlated; (ii) the source galaxy distribution somehow traces the matter field; (iii) the redshift distribution of source galaxies is rather broad. The width of the distribution depends on the source selection criterion, and generally the distribution of source galaxies overlaps with the distribution of lensing structures, so source galaxies are somehow correlated with the lensing potential. This correlation causes systematic effects on measurements of cosmic shear, which may be illustrated as follows. Fig. 1 shows a distribution of sources (denoted by filled circles) and the gravitational potential (contour lines). For line of sight 1 (LOS 1), the distant galaxies are lensed by the gravitational potential located at an intermediate distance and thus have a high *positive* lensing convergence.[2] This high signal is reduced by the excess of foreground sources bound to the foreground gravitational potential which, in contrast, has a low lensing. On the other hand, for a line of sight 2 (LOS 2), distant sources are lensed by the foreground void and thus have a *negative* lensing convergence. This negative signal is amplified because of the lack of foreground sources in the void. Accordingly, the probability distribution function of the lensing convergence, which is skewed toward a high value in the absence of SLC (e.g. BvWM97; Jain et al. 2000), becomes more symmetric than for the case of a random distribution of source galaxies. As a result, the amplitude of skewness of the lensing convergence drops.

As was pointed out by B98, there is another possible effect caused by intrinsic clustering of source galaxies. The average distance of sources and their sky density may indeed vary from one direction to another, which can cause additional systematic effects on the cosmic shear statistics (these effects were included in the definition of source clustering used by B98). It was pointed out by B98 and Thion et al. (2001) that this effect on the convergence skewness is in general very small. Therefore, in this analysis, we do not take it into account for the analytical calculations presented in the next section, although it will obviously be present in the numerical experiments discussed in Section 6.

3 THE PERTURBATION THEORY APPROACH

3.1 The quasi-linear regime

The expressions for the skewness of lensing convergence and the correlation term arising from SLC were first derived by BvWM97 and B98 in the framework of perturbation theory. In this subsection, we only summarize expressions that are directly relevant to this paper. Detailed derivations and notations are given in Appendix A.

In the presence of the SLC, the skewness parameter, defined by $S_3(\theta) = \langle\kappa_\theta^3\rangle/V_\kappa^2(\theta)$, consists of two terms: one arises from the

[2] The lensing convergence is not a direct observable but is obtained via a convergence reconstruction technique (Van Waerbeke, Bernardeau & Mellier 1999) or the aperture mass (Schneider et al. 1998) from a lensing shear map.

quasi-linear theory and the other from SLC:

$$S_3(\theta) = S_3^{\rm q.l.}(\theta) + S_3^{\rm slc}(\theta), \tag{1}$$

with

$$S_3^{\rm q.l.}(\theta) = \frac{\langle \kappa_\theta^3 \rangle^{\rm q.l.}}{V_\kappa^2(\theta)}$$
$$= \frac{6}{V_\kappa^2(\theta)} \left(\frac{H_0}{c}\right)^3 \int_0^{\chi_{\rm H}} {\rm d}\chi w^3(\chi)$$
$$\times \left[\frac{6}{7} I_0^2(\chi,\theta) + \frac{1}{4} I_0(\chi,\theta) I_1(\chi,\theta)\right], \tag{2}$$

$$S_3^{\rm slc}(\theta) = \frac{\langle \kappa_\theta^3 \rangle^{\rm slc}}{V_\kappa^2(\theta)}$$
$$= \frac{9\Omega_{\rm m}}{V_\kappa^2(\theta)} \left(\frac{H_0}{c}\right)^3 \int_0^{\chi_{\rm H}} {\rm d}\chi n_{\rm s}(\chi) b(\chi) w(\chi) I_0(\chi)$$
$$\times \int_0^{\chi} {\rm d}\chi' g(\chi',\chi) w(\chi') I_0(\chi')$$
$$- \frac{6}{V_\kappa(\theta)} \frac{H_0}{c} \int_0^{\chi_{\rm H}} {\rm d}\chi n_{\rm s}(\chi) b(\chi) w(\chi) I_0(\chi). \tag{3}$$

In these equations, θ is the size of the smoothing window, H_0/c is the Hubble constant in speed of light units, $V_k(\theta)$ is the variance of the lensing convergence [given by equation (A12)], χ denotes the radial comoving distance (and $\chi_{\rm H}$ corresponds to the horizon), $w(\chi)$ is the lensing efficiency function [equation (A8)], functions $I_0(\chi,\theta)$ and $I_1(\chi,\theta)$ depend on the power spectrum of matter density fluctuations through equations (A13) and (A16), $\Omega_{\rm m}$ is the matter density in units of the critical density, $n_{\rm s}\chi(z)$] the average number density of sources, function $g(\chi_{\rm l},\chi_{\rm s})$ is given by equation (A5), $b(\chi)$ is the linear biasing function between the galaxy and the matter density contrast.

3.2 Non-linear regime

For the variance of the lensing convergence, the effect of non-linear evolution of the density power spectrum can be included by replacing the linear power spectrum [which enters the above expressions through $V_\kappa(\theta)$, $I_0(\chi)$ and $I_1(\chi)$: see Appendix A for their explicit expressions] with the non-linear power spectrum, i.e. $P_{\rm lin}(a,k) \rightarrow P_{\rm NL}(a,k)$ (Jain & Seljak 1997). We use the fitting formula of the non-linear power spectrum given by Peacock & Dodds (1996). This semi-analytic approach has been tested against ray-tracing simulations, and a good agreement between the numerical results and the semi-analytic predictions has been found (Jain et al. 2000; White & Hu 2000).

In the framework of perturbation theory, all density contrasts needed for the calculation of the skewness correction term [equation (3)] correspond to linear order (see B98 for details). This comes from the fact that the quantity to be computed, an angular average of projected fourth moments, is given by the product of two two-point correlations: its intrinsic connected part has a negligible contribution because of the projection effects. The incorporation of the non-linear effects is then straightforward. As for the variance, it amounts to formally replacing the linear power spectrum with the non-linear one.

The semi-analytic calculation of the skewness in the non-linear regime was developed by Van Waerbeke et al. (2001b). It is based on the fitting formula of the density bispectrum by Scoccimarro & Couchman (2001) and is given by

$$S_3^{\rm n.l.}(\theta) = \frac{1}{V_\kappa^2(\theta)} \frac{6}{(2\pi)^4} \left(\frac{H_0}{c}\right)^3 \int_0^{\chi_{\rm max}} {\rm d}\chi w^3(\chi)$$
$$\times \int {\rm d}^2\boldsymbol{k}_1 P_{\rm NL}(k_1) W[k_1 f(\chi)\theta]$$
$$\times \int {\rm d}^2\boldsymbol{k}_2 P_{\rm NL}(k_2) W[k_2 f(\chi)\theta] \times W[|\boldsymbol{k}_1$$
$$+ \boldsymbol{k}_2| f(\chi)\theta] F_2^{\rm eff}(\boldsymbol{k}_1,\boldsymbol{k}_2), \tag{4}$$

with

$$F_2^{\rm eff}(\boldsymbol{k}_1,\boldsymbol{k}_2) = \frac{5}{7} a(n,k_1) a(n,k_2) + \frac{1}{2} b(n,k_1) b(n,k_2)$$
$$\times \frac{\boldsymbol{k}_1\cdot\boldsymbol{k}_2}{k_1 k_2} \left(\frac{k_1}{k_2} + \frac{k_2}{k_1}\right) + \frac{2}{7} c(n,k_1) c(n,k_2)$$
$$\times \frac{(\boldsymbol{k}_1\cdot\boldsymbol{k}_2)^2}{|k_1|^2 |k_2|^2}. \tag{5}$$

Here, the notations are as follows: $k = |\boldsymbol{k}|$, $f(\chi)$ denotes the comoving angular diameter distance (see Appendix A), W is the Fourier transform of the smoothing window, functions $a(n,k)$, $b(n, k)$ and $c(n, k)$ depend on the effective power spectral index n at scale k [explicit expressions are given by Scoccimarro & Couchman (2001); see also Van Waerbeke et al. (2001b)].

It should be noted that, since the bispectrum fitting formula is constructed via the dark matter bispectrum measured from only one N-body simulation data set, there is about a 10–20 per cent uncertainty in the fitting formula. This is mainly a cosmic variance effect (Van Waerbeke et al. 2001b).

4 MODELS

4.1 Cold dark matter models

We discuss three cold dark matter (CDM) models: a flat model with (ΛCDM) and without (SCDM) a cosmological constant, and an open model (OCDM), using galaxy cluster abundances to normalize the power spectrum (Eke, Cole & Frenk 1996; Kitayama & Suto 1997) and the formula of Bond & Efstathiou (1984) for the transfer function. The parameters of the models are listed in Table 1.

Table 1. Cosmological parameters for the models considered in this paper. $\Omega_{\rm m}$ is the matter density in units of the critical density, and similarly for the cosmological constant Ω_λ; $h \equiv H_0/100$ is the Hubble constant in units of $100\,{\rm km\,s^{-1}}$-Mpc^{-1}; σ_8 is the variance of the dark matter distribution in a sphere of radius $8\,h^{-1}$ Mpc.

Model	$\Omega_{\rm m}$	Ω_λ	h	σ_8
SCDM	1.0	0.0	0.5	0.6
OCDM	0.3	0.0	0.7	0.85
ΛCDM	0.3	0.7	0.7	0.9

4.2 Redshift distribution of source galaxies

We assume that $n_s(z)$ takes the form

$$n_s(z)\,dz = \frac{dz\beta}{z_*\Gamma[(1+\alpha)/\beta]}\left(\frac{z}{z_*}\right)^{\alpha}\exp\left[-\left(\frac{z}{z_*}\right)^{\beta}\right], \quad (6)$$

where $\Gamma(x)$ is the Gamma function.

We explore 12 models for the shape of the distribution. The parameters in each model are listed in Table 2. The average redshift is $\langle z\rangle = 1.2$, 1.5 and 0.9 for models A1–4, B1–4 and C1–4, respectively. We characterize the width of the distribution by the root-mean-square, Δz, which varies within a factor of $\simeq 3.2$, 3.5 and 3.2 in models A1–4, B1–4 and C1–4, respectively. Note that only model A1 matches roughly the observed redshift distribution of galaxies in current cosmic shear detections (Van Waerbeke et al. 2000). However, to keep our approach as general as possible, we still use a reasonably large parameter range for the possible shapes of the distributions.

Fig. 2 shows the redshift distribution of sources and the corresponding lensing efficiency as functions of redshift. In the top panel, SCDM is supposed, and various models for galaxy number counts are taken. In the bottom panel, model A1 is assumed for number counts, and various cosmologies are considered. Roughly speaking, the amplitude of SLC is controlled by the amplitude of overlapping between the population of sources $[n_s(z)]$ and that of lenses [which is very closely related to $w(z)/\Omega_m$]. It is important to keep in mind that the normalized efficiency function $w(z)/\Omega_m$ increases from SCDM to OCDM and then to ΛCDM.

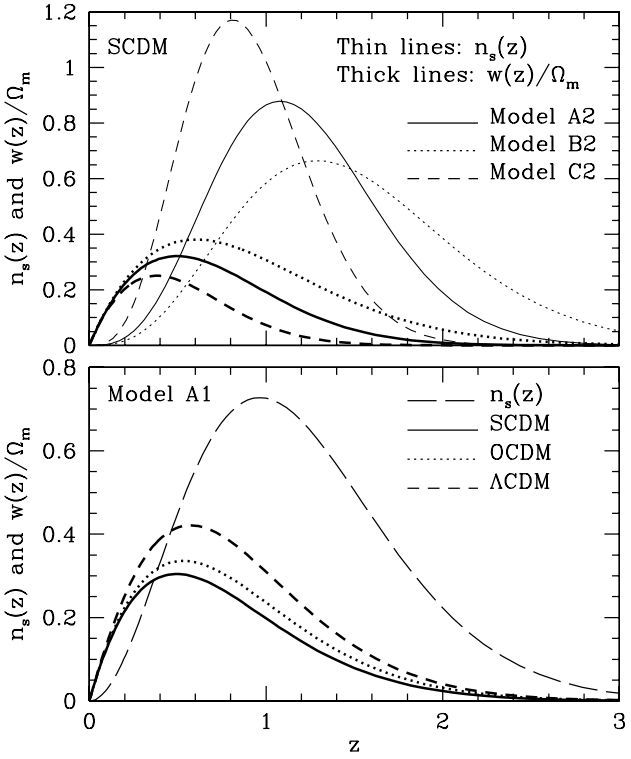

Figure 2. The redshift distributions of sources, $n_s(z)$, and the corresponding lensing efficiency functions divided by the density parameter, $w(z)/\Omega_m$, as functions of redshift. Top panel: for three source distribution models in the SCDM model. Bottom panel: for the A1 model in three cosmologies.

4.3 Model for the bias

We assume that the bias between the galaxy and the matter distribution is linear and takes a power-law form as a function of redshift, i.e.

$$b(z) = b_0(1+z)^{\gamma}. \quad (7)$$

We examine three cases, $\gamma = 0$, 1 and 2, and we take $b_0 = 1$. Since, so far, little is known about a realistic description of the bias, we adopt this model for its simplicity and the wide possible range of possibilities that it nevertheless covers. Numerical studies of dark matter clustering combined with measurements of the two-point correlation function in galaxy catalogues suggest that b_0 is close to unity (e.g. Jenkins et al. 1998).

Table 2. Parameters in $n_s(z)$.

Model	$\langle z\rangle$	Δz	α	β	z_*
A1	1.2	0.572	2	1.5	0.798
A2	1.2	0.456	3	1.8	0.813
A3	1.2	0.297	5	3.0	1.01
A4	1.2	0.182	8	6.0	1.18
B1	1.5	0.866	2	1.0	0.500
B2	1.5	0.618	3	1.5	0.812
B3	1.5	0.400	5	2.5	1.11
B4	1.5	0.244	7	6.0	1.51
C1	0.9	0.429	2	1.5	0.598
C2	0.9	0.342	3	1.8	0.610
C3	0.9	0.240	5	2.5	0.667
C4	0.9	0.136	8	6.0	0.884

5 RESULTS

Let us introduce the parameter that characterizes the amplitude of the SLC effects defined by

$$R = -\frac{S_3^{\rm slc}}{S_3}, \quad (8)$$

where $S_3^{\rm slc}$ is the correction brought by SLC and S_3 is the skewness in the case of the absence of SLC ($S_3^{\rm q.l.}$ and $S_3^{\rm n.l.}$ for quasi-linear and non-linear computations, respectively).

Fig. 3 shows S_3 (upper panel), with and without taking the SLC effect into account, and R (lower panel) as a function of θ for the A1 model and SCDM. Non-linear effects on the skewness are discussed in detail by Van Waerbeke et al. (2001b). It should be noted that non-linear growth of the density field enhances the skewness significantly at scales below 1°, so the SLC correction term remains relatively small because of cancellations between the numerator and the denominator in the first line of equation (3) (see also Appendix A for the explicit expressions for V_κ and $S_3^{\rm slc}$). As a consequence, R decreases significantly when $\theta < 20$–30 arcmin. It should be also noted that for $\theta \gtrsim 100$ arcmin, where non-linear effects can be safely neglected, the SLC effect is reduced while θ increases. This is due to the change in the slope of the density power spectrum occurring when the spatial smoothing scale $f(\chi)\theta$ at $z = 0.3$–0.8, from where the most of the lensing contribution comes, is of the order of $10(\Omega_m h^2)^{-1}$ Mpc.

Let us now discuss the theoretical predictions that take into account non-linear effects. Fig. 4 shows S_3 and R for three cosmologies (top panel) and three bias evolution models (bottom panel). The top panel clearly shows that it is essential to take SLC

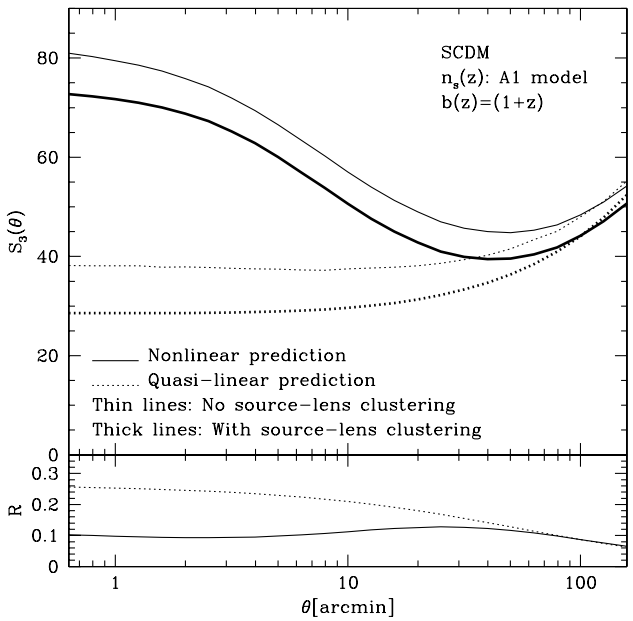

Figure 3. Upper panel: predicted skewness of the lensing convergence for A1 and SCDM, with and without the source clustering effect taken into account. Lower panel: the ratio R as defined in equation (8).

into account to put constraints on values of $\Omega_{\rm m}$ determined from S_3. Fig. 4 also suggests that SLC is more important for low- than for high-density models. This is explained by the fact that the efficiency function is larger in the first than in the second case, as illustrated by Fig. 2. The bottom panel of Fig. 4 also shows that the SLC effect increases with strength of evolution in bias with redshift. This is a natural consequence of the fact that the SLC effect is caused by the correlation between the lensing potential (the matter distribution) and the distribution of source galaxies. Finally, note that for $\theta \lesssim 10$ arcmin, the relative SLC effect is nearly independent of scale.

Figs 3 and 4 show that the relative SLC effect, R, peaks around $\theta = 30$–60 arcmin. One might wonder what should be the ideal smoothing scale for measuring the skewness while reducing the SLC effect as much as possible: should it be larger or smaller than the peak position? To answer this question properly, one also has to consider the signal-to-noise ratio, *S/N*. Typically, the signal-to-noise ratio in S_3 is expected to decrease with θ because of the finite area covered by the survey. Van Waerbeke et al. (1999) numerically investigated the efficiency of weak lensing surveys, taking into account both this effect and the noise arising from the intrinsic ellipticity of the source galaxies. Figs 8 and 10 of their paper indicate that it might be difficult to detect the skewness with $S/N > 1$ at smoothing scales larger then 60 arcmin, even with a wide field survey covering $10^\circ \times 10^\circ$. This suggests that the best choice for the smoothing scale, keeping both SLC effects low and a good signal-to-noise ratio, should be θ of the order of 1 arcmin.[3]

Fig. 5 shows R for $\theta = 1$ arcmin (left-hand panels) and 10 arcmin (right-hand panels) as a function of the source redshift distribution width, Δz. A comparison of the left- and right-hand panels confirms a visual inspection of Fig. 4, namely that R is fairly insensitive to θ in the scaling regime considered, $\theta \lesssim 10$ arcmin.

[3] It should be noted, however, that to break the degeneracy between cosmological parameters, one still has to measure cosmic shear statistics at linear scales, i.e. $\theta > 1^\circ$ (Jain & Seljak 1997).

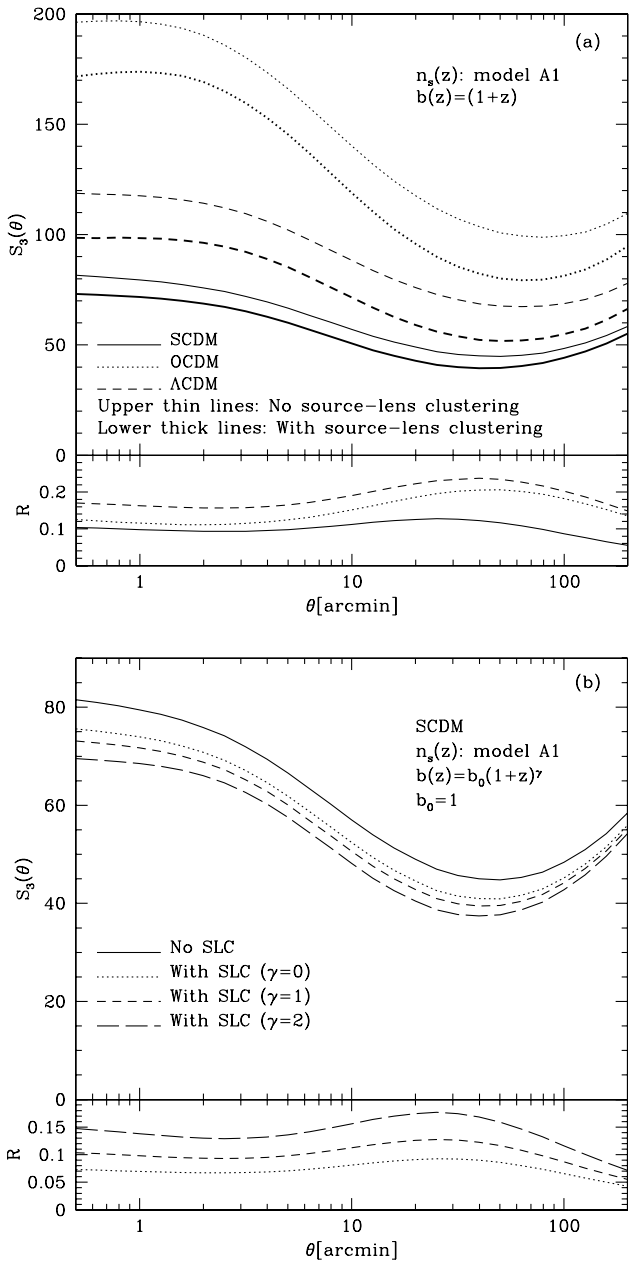

Figure 4. S_3 and R [equation (8)] with and without the source clustering effect taken into account as functions of scale. The non-linear ansatz is used. Cosmology and source distribution models are denoted in each plot: (a) three different cosmological models are considered; (b) three different bias evolution models are considered.

The top and bottom panels indicate that effects of the cosmology and bias evolution model on the amplitude of parameter R are significant, but the shape of R as a function of Δz remains fairly stable. Note furthermore that, in the middle panels, models with the same mean source redshift form sequences in the Δz–R plane with very similar slopes at fixed Δz.

This suggests that, for a choice of the cosmological model and γ, there exists a simple phenomenological law that relates R to $\langle z \rangle$ and Δz, which is valid for all source models considered here,

$$R = A \frac{\Delta z^C}{\langle z \rangle^B}, \tag{9}$$

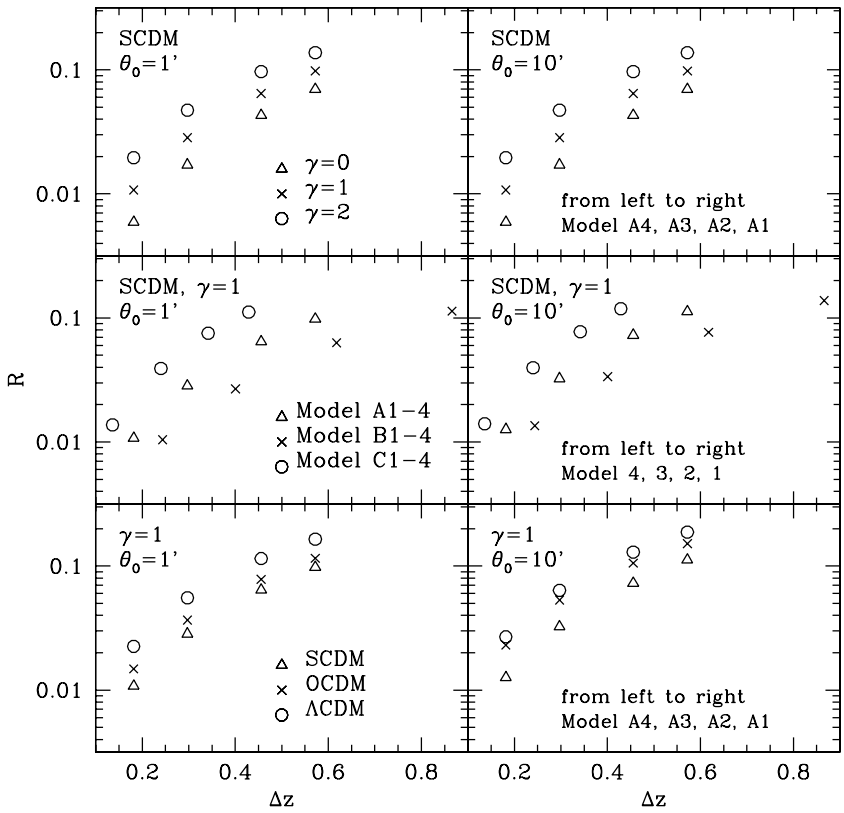

Figure 5. R as a function of Δz as predicted from our semi-analytic model. The smoothing scales are 1 and 10 arcmin for the left- and right-hand panels, respectively. The top panels are for three bias models in SCDM, A1–4; the middle panels are for all 12 source distribution models in the SCDM $\gamma = 1$ case; and the bottom panels are for three cosmological models in the $\gamma = 1$ A1–4; cases.

where A is of the order of 0.5, B and C varying from 1.5 to 3. The precise values of parameters (A, B, C) are obtained by a least-squares fitting method. They are given in Table 3.

The accuracy of this law is demonstrated in Fig. 6. One can see that the data lie fairly well on the parametrized line. This allows us to make a contour plot of parameter R in $\langle z\rangle - \Delta z$ space, as shown in Fig. 7, for three cosmological models. Not surprisingly, this figure clearly indicates that the way to reduce the SLC effect on a measurement of the skewness is to make the source distribution narrow with a high mean redshift.

Finally, we examine the dependence of the SLC effect on the evolution of bias. Fig. 8 shows R as a function of γ for four models selected arbitrarily. For each source distribution model, the $R-\gamma$ relation is well fitted by the following empirical law:

$$\log R = \epsilon\gamma + \text{constant} \tag{10}$$

The coefficient ϵ, which describes the strength of the dependence of the SLC effect on the evolution of bias, is shown in Fig. 9 as a function of $R(\gamma = 1)$ for all source distribution models that we consider. Each panel corresponds to a given choice of cosmology. One can see that ϵ remains in the range $0.1 < \epsilon < 0.3$ and is almost insensitive to both smoothing scale and cosmology. At a fixed value of $R(\gamma = 1)$, ϵ increases with mean redshift (in the order C, A, B). This is a natural consequence of the fact that, for our choice of the bias evolution model equation (7), the impact of the change in the bias evolution is more significant at a higher redshift.

The uncertainty in parameter R caused by our ignorance of $b(z)$ can be roughly estimated using the empirical relation (10) as follows: suppose that the power-law model (7) for the evolution of bias stands, but that there is an error Δ_γ on the value of γ. Applying simple error propagation techniques, one finds $\delta R/R = 2.3\epsilon\Delta_\gamma (\sim 0.5\Delta_\gamma)$: if one is able to constrain the bias evolution model with an accuracy better than $\Delta_\gamma < 0.4$, the uncertainty in R drops below 20 per cent.

Table 3. Parameters of the phenomenological law [equation (9)] derived from semi-analytic calculations.

		$\theta = 1$ arcmin			$\theta = 10$ arcmin		
	γ	A	B	C	A	B	C
SCDM	$\gamma = 0$	0.56	3.0	2.5	0.58	2.9	2.4
	$\gamma = 1$	0.62	2.7	2.2	0.64	2.6	2.1
	$\gamma = 2$	0.70	2.4	1.9	0.72	2.3	1.8
OCDM	$\gamma = 0$	0.59	2.8	2.3	0.43	2.1	1.8
	$\gamma = 1$	0.66	2.5	2.0	0.72	2.3	1.8
	$\gamma = 2$	0.50	1.7	1.5	0.80	2.1	1.6
ΛCDM	$\gamma = 0$	0.65	2.6	2.1	0.67	2.5	2.0
	$\gamma = 1$	0.72	2.4	1.8	0.75	2.2	1.7
	$\gamma = 2$	0.81	1.8	1.6	0.84	1.9	1.4

6 TESTING SEMI-ANALYTIC PREDICTIONS AGAINST NUMERICAL SIMULATIONS

In this section, we compare theoretical predictions with ray-tracing experiments in N-body simulations, using mock galaxy catalogues extracted from the simulations as distributions of sources. The

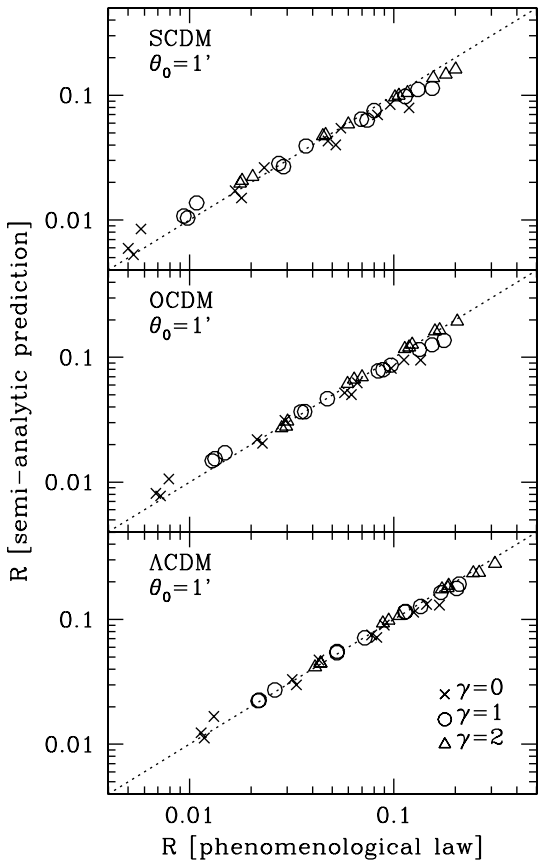

Figure 6. R computed by the semi-analytic formula versus that derived from the phenomenological law [equation (9)]. The parameters (A, B, C) for each case are summarized in Table 3.

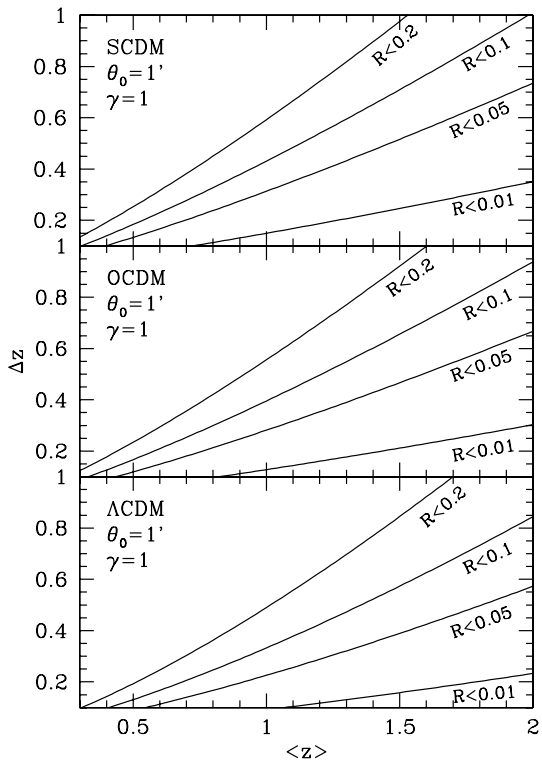

Figure 7. Contour lines of R obtained from our semi-analytic modeling in the $\langle z\rangle$–Δz plane for $\theta = 1$ arcmin and $\gamma = 1$. Each panel corresponds to a different cosmology.

N-body data sets and the ray-tracing method used for this work are described in Appendix B. In Appendix C, details of the procedure to generate mock galaxy catalogues are presented. We focus only on the SCDM model, but the conclusions of our numerical analysis should not depend significantly on the cosmology considered.

We measure convergence statistics on mock galaxy catalogues as follows. The value of convergence for a galaxy at redshift z is given by linear interpolation between the κ_i – computed from rays propagating between redshift z of the closest lens plane to the galaxy (see Appendix B) and the present time – measured at the four nearest angular pixels from the galaxy position in the sky. The amplitude of the SLC effect is measured by comparing simulations with similar SLC-free ones. They are obtained from other mock galaxy catalogues with the same source distribution $n_s(z)$ (i.e. the same as in the SLC mock catalogue), in which galaxies are randomly distributed on the sky. Note finally that top hat filtering is used and the intrinsic ellipticity of galaxies is not taken into account.

The upper panel of Fig. 10 shows the skewness parameter measured from the $\gamma = 0$ mock galaxy catalogue with and without the SLC effect. The lower panel displays the function $R(\theta)$, except that in the denominator of equation (8), we always take the value given by non-linear semi-analytic predictions, $S_3^{\rm n.l.}$. As discussed in Appendix B (see also Hamana & Mellier 2001), the simulations have limited available dynamic range since they are contaminated by force softening and finite volume effects at small and large scales respectively, where the measured S_3 is expected to underestimate the real value. Furthermore, there is a 10–20 per cent uncertainty in the non-linear perturbation theory predictions. With these elements in mind, we see that agreement between measurements and predictions is reasonable when SLC effects are taken into account. In particular, the order of magnitude of the shift between the upper and lower symbols in the top panel of Fig. 10 matches very well that between the dotted and solid curves, as illustrated by bottom panel.

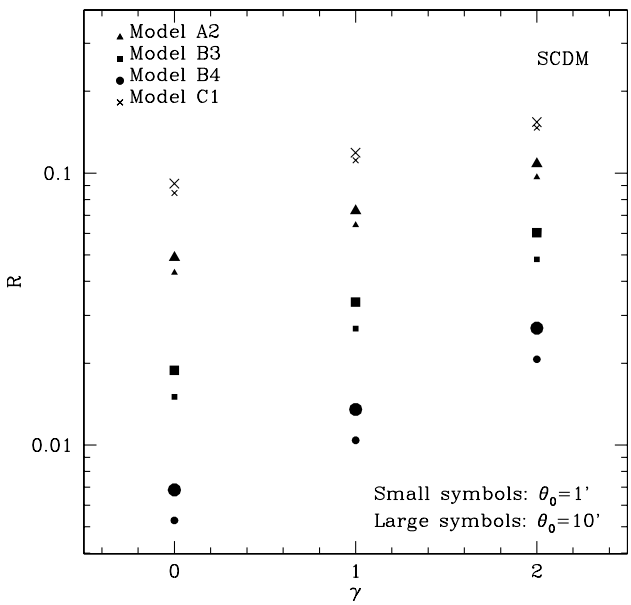

Figure 8. Semi-analytic values of R as a function of γ for four selected models in SCDM.

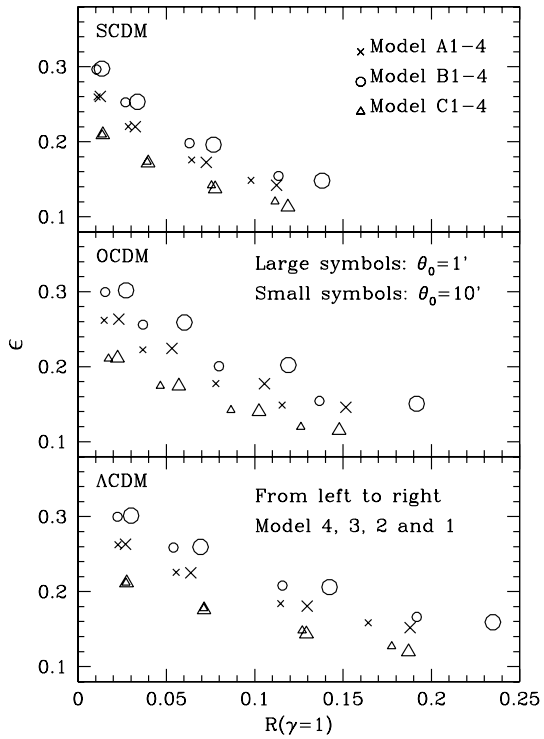

Figure 9. The slopes of the $R-\gamma$ relation in the semi-analytic model. Coefficient ϵ as defined in equation (10) is shown as a function of $R(\gamma = 1)$.

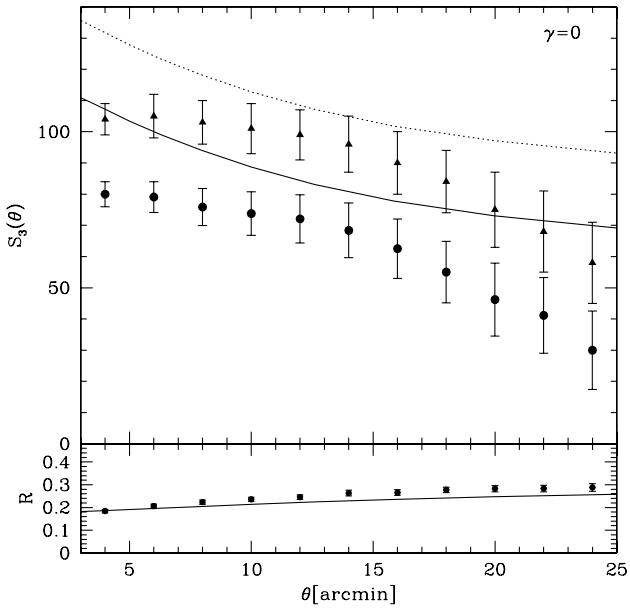

Figure 10. S_3 (upper panel) and R (lower panel) as functions of the smoothing angle θ in the $\gamma = 0$ case. The solid (dotted) line shows the semi-analytic prediction with (without) the SLC effect taken into account, while the filled circles (triangles) show the results of ray-tracing simulations with (without) the SLC effect taken into account. Error bars give some estimate of the uncertainty E on the measurements, i.e. $E(S_3) \simeq \Delta S_3/\sqrt{40}$, where $(\Delta S_3)^2$ is the dispersion over the 40 realizations. Note that R is calculated as $R = -S_3^{\rm slc}/S_3^{\rm n.l.}$, where $S_3^{\rm n.l.}$ is always given by semi-analytic predictions.

Similar results are obtained for the $\gamma = 1$ and 2 catalogues, as summarized in Fig. 11, which concentrates on the parameter R. Since numerical experiments for $\gamma = 1$ and 2 cases are done with threshold bias instead of the linear bias used in the semi-analytic computation, we should only focus on the differences among the three models arising from different evolution of biasing. Although there is a systematic difference between the predictions and measurements, a trend in the dependence of evolution of biasing on the SLC effect found in the predictions is well reproduced in the measurements.

Furthermore, one finds that the $\gamma = 2$ measurement agrees better with the $\gamma = 3$ prediction except for the largest angular scales. This is consistent with the scale dependence of biasing detected in the $\gamma = 2$ mock catalogue (on small scales the bias evolves as $\gamma = 3$: see Appendix C for detailed discussion on this point). We may conclude from the results above that the semi-analytic approach gives a good prediction of the SLC effect on the convergence skewness.

7 SUMMARY AND DISCUSSION

We have examined the source–lens clustering (SLC) effect on measurements of the skewness of lensing convergence using a non-linear semi-analytic approach. The results of semi-analytic predictions have been tested against numerical simulations, and a good agreement between them has been found. Our main conclusions are as follows.

(i) The SLC effect strongly depends on the redshift distribution of source galaxies. We find that the effect scales with the width and mean redshift of the distribution roughly as $R \propto \langle z \rangle^{-(3.0-1.8)} \Delta z^{1.4-2.5}$ (where $R = -S_3^{\rm slc}/S_3$, and $S_3^{\rm slc}$ is the change in measured S_3 due to SLC). As illustrated by Fig. 7, this relation indicates that it is essential to make the width of the distribution small and its mean redshift high to reduce the SLC effect (this was partly pointed out by B98).

(ii) The SLC effect also depends on the evolution of the bias

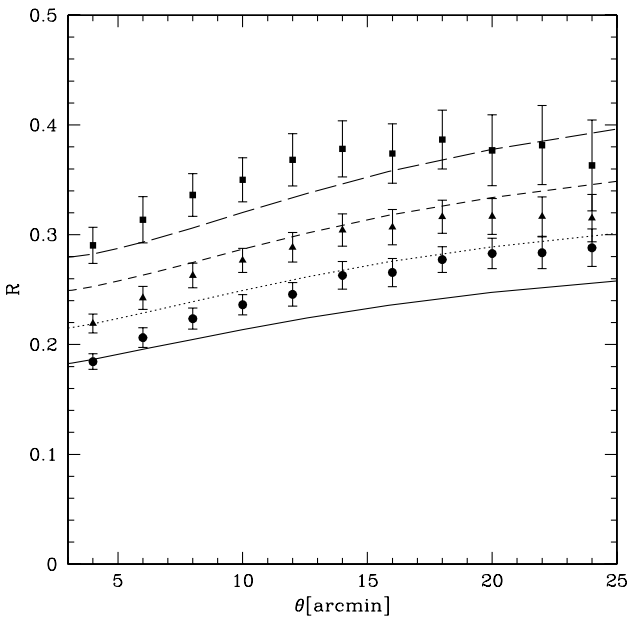

Figure 11. The parameter R as displayed in the lower panel of Fig. 10 but now for all values of γ considered. Symbols show the results of ray-tracing simulations: circles, triangles and squares correspond respectively to $\gamma = 0$, 1 and 2 mock catalogues. Lines correspond to semi-analytical predictions, $\gamma = 0$, 1, 2, 3 from bottom to top. Error bars are computed as explained in the caption of Fig. 10.

between the galaxy and total matter distributions, $b(z)$. Assuming a simple power-law model and linear bias, $b(z) \propto (1+z)^{\gamma}$, we find that the uncertainty in γ transforms into $\delta R/R = 2.3\epsilon\Delta_{\gamma}$ with a typical value of $\epsilon \sim 0.2$. This indicates that the uncertainty in γ must be $\Delta_{\gamma} < 0.2$ to predict the amplitude of the SLC effect with better than 10 per cent accuracy.

The main uncertainty in semi-analytic predictions comes from the fact that the accuracy of the non-linear fitting formula of the density bispectrum is only 10–20 per cent. We expect the same level of uncertainty in predictions presented in this paper for the SLC effect on the convergence skewness. This can actually be improved by measurements in large N-body simulations with high spatial resolution.

Since, so far, little is known about the evolution of the bias, it is still very difficult to predict the SLC effect accurately. It is therefore very important to reduce this effect as much as possible by controlling the redshift distribution of sources. The above results tells us that an ideal observational strategy might be as follows: (i) going to a deep limiting magnitude to increase the mean redshift of the survey; and (ii) using only faint images to reduce the width of the distribution. A desirable source distribution for $R < 0.1$ suggested by Fig. 7 would have $\Delta z < 0.3$ and $\langle z \rangle > 1$. This may of course be challenging: going to deeper magnitudes will make the calculation of the redshift distribution of sources more difficult, and using only faint images will increase the noise arising from the intrinsic ellipticity of galaxies. We leave more detailed studies on the design of optimal strategies to future works.

Before closing this paper, it is important to emphasize that the use of source galaxies with a small redshift width may unfortunately introduce additional skewness signal owing to the intrinsic correlation of galaxy ellipticities. It was indeed suggested that the amplitude of this latter effect scales roughly as $(\Delta z)^{-1}$, although the normalization of this relation is ambiguous because of the uncertainty in the correlation between the shape of galaxies and that of their dark matter haloes (Heavens, Refregier & Heymans 2000; Pen, Lee & Seljak 2000; Croft & Metzler 2001; Crittenden et al. 2001; Catelan, Kamionkowski & Blandford 2001; Hatton & Ninin 2001). However, as pointed out by Croft & Metzler (2001), intrinsic ellipticity correlations might just act as an additional source of random noise, without significantly influencing the measured value of the skewness of the convergence.

ACKNOWLEDGMENTS

We thank L. Van Waerbeke for providing the FORTRAN code to compute the non-linear skewness of convergence, and for helpful comments. We also thank A. Stebbins for teaching us his way of generating mock galaxy catalogues from N-body simulations, and S. Hatton for very useful suggestions to improve the text. This research was supported in part by the Direction de la Recherche du Ministère Fran¸cais de la Recherche. The computational means (CRAY-98 and NEC-SX5) to do the N-body simulations were made available to us thanks to the scientific council of the Institut du Développement et des Ressources en Informatique Scientifique (IDRIS). Numerical computation in this work was partly carried out at IAP at the TERAPIX data centre and on MAGIQUE (SGI-02K).

REFERENCES

Bacon D., Refregier A., Ellis R., 2000, MNRAS, 318, 625
Bartelmann M., Schneider P., 2001, Phys. Rep., 340, 291
Bernardeau F., 1998, A&A, 338, 375, (B98)
Bernardeau F., Van Waerbeke L., Mellier Y., 1997, A&A, 322, 1, (BvWM97)
Bond J. R., Efstathiou G., 1984, ApJ, 285, L45
Catelan P., Kamionkowski M., Blandford R. D., 2001, MNRAS, 320, L7
Colombi S., Bouchet F. R., Schaeffer R., 1994, A&A, 281, 301
Colombi S., Szapudi I., Szalay A. S., 1998, MNRAS, 296, 253
Crittenden R. G., Natarajan P., Pen U.-L., Theuns T., 2001, ApJ, 559, 552
Croft R. A. C., Metzler C. A., 2001, ApJ, 545, 561
Devriendt J. E. G., Guiderdoni B., 2000, A&A, 363, 851
Eke V. R., Cole S., Frenk C. S., 1996, MNRAS, 282, 263
Hamana T., 2001, MNRAS, 326, 326
Hamana T., Mellier Y., 2001, MNRAS, 327, 169
Hamana T., Colombi S., Suto Y., 2001, A&A, 367, 18
Hatton S., Ninin S., 2001, MNRAS, 322, 576
Heavens A., Refregier A., Heymans C., 2000, MNRAS, 319, 649
Jain B., Seljak U., 1997, ApJ, 484, 560
Jain B., Seljak U., White S. D. M., 2000, ApJ, 530, 547
Jenkins A. et al., 1998, ApJ, 499, 20, (The Virgo Consortium)
Kaiser N., 1992, ApJ, 388, 272
Kaiser N., Wilson G., Luppino G. A., 2000, ApJ, submitted (astro-ph/0003338)
Kitayama T., Suto Y., 1997, ApJ, 490, 557
Maoli R. et al., 2001, A&A, 368, 766
Mellier Y., 1999, ARA&A, 37, 127
Peacock J. A., Dodds S. J., 1996, MNRAS, 280, L19
Pen U.-I., Lee J., Seljak U., 2000, ApJ, 543, L107
Schneider P., Van Waerbeke L., Jain B., Kruse G., 1998, MNRAS, 296, 873
Scoccimarro R., Couchman H. M. P., 2001, MNRAS, 325, 1312
Seto N., 1999, ApJ, 523, 24
Thion A., Mellier Y., Bernardeau F., Bertin E., Erben T., Van Waerbeke L., 2001, in Kneib J.-P., Mellier Y., Moniez M., Tran Thanh Van J., eds, Proc. XXth Moriond Astrophysics Meeting, Cosmological Physics with Gravitational Lensing. EDP Sciences, Les Ulis, p. 191
Van Waerbeke L., Bernardeau F., Mellier Y., 1999, A&A, 342, 15
Van Waerbeke L. et al., 2000, A&A, 358, 30
Van Waerbeke L. et al., 2001a, A&A, 374, 757
Van Waerbeke L., Hamana T., Scoccimarro R., Colombi S., Bernardeau F., 2001b, MNRAS, 322, 918
White M., Hu W., 2000, ApJ, 537, 1
Wittman D. N., Tyson J. A., Kirkman D., Dell'Antonio I., Bernstein G., 2000, Nat, 405, 143

APPENDIX A: PERTURBATION THEORY APPROACH TO THE COSMIC SHEAR STATISTICS IN THE PRESENCE OF SLC

The expressions for the skewness of lensing convergence and the correlation term arising from SLC were first derived by BvWM97 and B98, respectively, in the framework of perturbation theory. However, B98 only gave the expression for the case of an Einstein–de Sitter cosmological model and assumed power-law density power spectrum. In this Appendix, to make this paper self-contained, we re-derive the skewness terms which are valid for an arbitrary Friedmann model. We basically follow the original deviation by B98. It should be noted that the skewness corrections not only are caused by the SLC but also arise from e.g. the lens–lens coupling (BvWM97; Van Waerbeke et al. 2001b) and the lensing magnification effect (Hamana 2001). In what follows, we focus on the SLC correction and are not concerned with other correction terms.

A1 Fluctuation in a source distribution due to the source clustering

The number density of sources at redshift z and in direction $\boldsymbol{\phi}$ can be written

$$n_{\rm s}^{\rm obs}[\chi(z),\boldsymbol{\phi}] = n_{\rm s}[\chi(z)]\{1+\delta_{\rm s}[\chi(z),\boldsymbol{\phi}]\}, \tag{A1}$$

where $n_{\rm s}[\chi(z)]$ is the average number density of sources, $\delta_{\rm s}[\chi(z),\boldsymbol{\phi}]$ is their local density contrast and χ denotes the radial comoving distance. We suppose, as B98, that the average source number density is normalized to unity, $\int_0^{\chi_{\rm H}} {\rm d}\chi n_{\rm s}(\chi)=1$, where $\chi_{\rm H}$ is the distance to the horizon (the normalized distribution denotes the probability distribution). Following B98, we assume that the density contrast of sources is related to the matter density contrast, δ, via the linear biasing,

$$\delta_{\rm s}(\chi,\boldsymbol{\phi}) = b(\chi)\delta(\chi,\boldsymbol{\phi}). \tag{A2}$$

A2 Convergence statistics in the presence of SLC

Let us consider the measured convergence that results from averages made over many distant galaxies located at different distances. Denoting the smoothing scale by θ, such an average can formally be written as

$$\kappa_\theta = \frac{\sum_{i=1}^{N_{\rm s}} W_\theta(\boldsymbol{\phi}_i)\kappa_{\rm s}(z_i,\boldsymbol{\phi}_i)}{\sum_{i=1}^{N_{\rm s}} W_\theta(\boldsymbol{\phi}_i)}, \tag{A3}$$

where $W_\theta(x)$ denotes the weight function of the average, $N_{\rm s}$ is the number of source galaxies, and $\kappa_{\rm s}(z_i,\boldsymbol{\phi}_i)$ is the lensing convergence signal from a source galaxy located at redshift z_i in a direction $\boldsymbol{\phi}_i$ and is given by (e.g. Mellier 1999; Bartelmenn & Schneider 2001)

$$\kappa_{\rm s}(z,\boldsymbol{\phi}) = \frac{3\Omega_{\rm m}}{2}\frac{H_0}{c}\int_0^{\chi_{\rm s}(z)} {\rm d}\chi_{\rm l} g(\chi_{\rm l},\chi_{\rm s})\delta(\chi_{\rm l},\boldsymbol{\phi}), \tag{A4}$$

with

$$g(\chi_{\rm l},\chi_{\rm s}) = \frac{H_0 f(\chi_{\rm l}) f(\chi_{\rm s}-\chi_{\rm l})}{c\, f(\chi_{\rm s}) a(\chi_{\rm l})}. \tag{A5}$$

Here a is the scalefactor normalized to its present value, and $f(\chi)$ denotes the comoving angular diameter distance, defined as $f(\chi)=K^{-1/2}\sin K^{1/2}\chi$, χ, $(-K)^{-1/2}\sinh(-K)^{1/2}\chi$ for $K>0$, $K=0$, $K<0$, respectively, where K is the curvature which can be expressed as $K=(H_0/c)^2(\Omega_{\rm m}+\Omega_\lambda-1)$. For the weight function, the angular top-hat filter (BvWM97) and/or compensated filter (Schneider et al. 1998) are commonly adopted (e.g. Van Waerbeke et al. 2001a). In what follows, we consider the top-hat filter for the weight function, and in this case equation (A3) is reduced to

$$\kappa_\theta = \sum_{i=1}^{N_s^j} \kappa_{\rm s}(z_i,\boldsymbol{\phi}_i)/N_s^j,$$

where N_s^j is the number of source galaxies within an aperture θ centred on a direction $\boldsymbol{\phi}_j$. The number density of sources for current and future weak lensing analyses is about 40 per arcmin^2 (e.g. Van Waerbeke et al. 2001a), which typically implies more than 100 galaxies in discs of radius $\theta \geq 1$ arcmin. As a result, discreteness effects from the source distribution can be neglected (see also B98) and we can rewrite (A3) in the continuous limit:

$$\kappa_\theta = \frac{\int {\rm d}^2\phi W_\theta(\boldsymbol{\phi})\int_0^{\chi_{\rm H}} {\rm d}\chi \kappa_{\rm s}(\chi,\boldsymbol{\phi}) n_s^{\rm obs}(\chi,\boldsymbol{\phi})}{\int d^2\phi W_\theta(\boldsymbol{\phi})\int_0^{\chi_{\rm H}} {\rm d}\chi n_s^{\rm obs}(\chi,\boldsymbol{\phi})}. \tag{A6}$$

Let us now expand equation (A6) in terms of δ using the perturbation theory approach, following BvWM97. The presence of SLC does not change the expression of the first-order term,

$$\begin{aligned}\kappa_\theta^{(1)} &= \frac{3\Omega_{\rm m}}{2}\frac{H_0}{c}\int {\rm d}^2\phi W_\theta(\boldsymbol{\phi})\int_0^{\chi_{\rm H}} {\rm d}\chi_{\rm s} n_{\rm s}(\chi_{\rm s}) \\ &\quad\times\int_0^{\chi_{\rm s}} {\rm d}\chi_{\rm l} g(\chi_{\rm l},\chi_{\rm s})\delta^{(1)}(\chi_{\rm l},\boldsymbol{\phi}) \\ &= \frac{H_0}{c}\int {\rm d}^2\phi W_\theta(\boldsymbol{\phi})\int_0^{\chi_{\rm H}} {\rm d}\chi_{\rm l} w(\chi_{\rm l})\delta^{(1)}(\chi_{\rm l},\boldsymbol{\phi}),\end{aligned} \tag{A7}$$

where $w(\chi)$ is the so-called the lensing efficiency function defined by

$$w(\chi_{\rm l}) = \frac{3\Omega_{\rm m}}{2}\int_{\chi_{\rm l}}^{\chi_{\rm H}} {\rm d}\chi_{\rm s} g(\chi_{\rm l},\chi_{\rm s}) n_{\rm s}(\chi_{\rm s}). \tag{A8}$$

The second-order convergence consists of two terms: one comes from the second-order density perturbation and it is formally written by replacing the subscript $^{(1)}$ in the first-order expression (A7) with $^{(2)}$ (BvWM97); the other one is due to SLC,

$$\begin{aligned}\kappa_\theta^{{\rm slc}(2)} &= \frac{3\Omega_{\rm m}}{2}\frac{H_0}{c}\int {\rm d}^2\phi W_\theta(\boldsymbol{\phi})\times\int_0^{\chi_{\rm H}} {\rm d}\chi n_{\rm s}(\chi) b(\chi)\delta^{(1)}(\chi,\boldsymbol{\phi}) \\ &\quad\times\int_0^{\chi} {\rm d}\chi' g(\chi',\chi)\delta^{(1)}(\chi',\boldsymbol{\phi}) - \kappa_\theta^{(1)}\int {\rm d}^2\phi W_\theta(\boldsymbol{\phi}) \\ &\quad\times\int_0^{\chi_{\rm H}} {\rm d}\chi n_{\rm s}(\chi) b(\chi)\delta^{(1)}(\chi,\boldsymbol{\phi}).\end{aligned} \tag{A9}$$

Using the small-angle approximation (Kaiser 1992), equation (A7) is rewritten in terms of the Fourier transform of the density contrast, $\delta(k)$, as

$$\begin{aligned}\kappa_\theta^{(1)} &= \frac{H_0}{c}\int_0^{\chi_{\rm H}} {\rm d}\chi w(\chi)\int\frac{{\rm d}^3k}{(2\pi)^3}\delta^{(1)}[\boldsymbol{k};\chi]\exp[{\rm i}k_\chi f(\chi)] \\ &\quad\times W[f(\chi)k_\perp\theta],\end{aligned} \tag{A10}$$

where the wave vector $\boldsymbol{k}$ is decomposed into the line-of-sight component k_χ and its perpendicular, $\boldsymbol{k}_\perp$, and $W(x)$ is the Fourier transform of the weight function. In the case of the top-hat filter, $W(x)=2J_1(x)/x$ where J_1 is the Bessel function of first order. In the same manner, equation (A9) reads

$$\begin{aligned}\kappa_\theta^{{\rm slc}(2)} &= \frac{3\Omega_{\rm m}}{2}\frac{H_0}{c}\int_0^{\chi_{\rm H}} {\rm d}\chi n_{\rm s}(\chi) b(\chi)\int_0^{\chi} {\rm d}\chi' g(\chi',\chi) \\ &\quad\times\int\frac{{\rm d}^3k}{(2\pi)^3}\delta^{(1)}[\boldsymbol{k};\chi]\exp[{\rm i}k_\chi f(\chi)] \\ &\quad\times\int\frac{{\rm d}^3k'}{(2\pi)^3}\delta^{(1)}[\boldsymbol{k}';\chi']\exp[{\rm i}k'_\chi f(\chi')]\times W[|f(\chi)\boldsymbol{k}_\perp \\ &\quad+f(\chi')\boldsymbol{k}'_\perp|\theta] - \kappa_\theta^{(1)}\int_0^{\chi_{\rm H}} {\rm d}\chi n_{\rm s}(\chi) b(\chi) \\ &\quad\times\int\frac{{\rm d}^3k}{(2\pi)^3}\delta^{(1)}[\boldsymbol{k};\chi]\exp[{\rm i}k_\chi f(\chi)]W[f(\chi)k_\perp\theta].\end{aligned} \tag{A11}$$

The average of the convergence is not affected by the presence of the SLC and is therefore zero, $\langle\kappa\rangle=0$. The variance is not

affected by it either at linear order, and is given by

$$V_\kappa(\theta) = \langle \kappa_\theta^{(1)2} \rangle = \left(\frac{H_0}{c}\right)^2 \int_0^{\chi_H} \mathrm{d}\chi_1 w^2(\chi_1) I_0(\chi_1, \theta), \tag{A12}$$

with

$$I_0(\chi, \theta) = \frac{1}{2\pi} \int \mathrm{d}k k P_{\rm lin}(\chi, k) W_{\rm 2D}^2[kf(\chi)\theta], \tag{A13}$$

where $P_{\rm lin}\chi(z),k]$ is the linear density power spectrum. In the presence of SLC, the skewness parameter, defined by $S_3(\theta) = \langle \kappa_\theta^3 \rangle / V_\kappa^2(\theta)$, consists of two terms. One comes from the second-order perturbation (BvWM97),

$$\langle \kappa_\theta^3 \rangle^{\rm q.l.} = 3 \langle \kappa_\theta^{(1)2} \kappa_\theta^{(2)} \rangle \tag{A14}$$

$$= 6 \left(\frac{H_0}{c}\right)^3 \int_0^{\chi_H} \mathrm{d}\chi w^3(\chi) \times \left[\frac{6}{7} I_0^2(\chi, \theta) + \frac{1}{4} I_0(\chi, \theta) I_1(\chi, \theta)\right], \tag{A15}$$

where

$$I_1(\chi, \theta) = \frac{1}{2\pi} \int \mathrm{d}k k^2 P_{\rm lin}(\chi, k) \frac{\mathrm{d}W_{\rm 2D}^2[kf(\chi)\theta]}{\mathrm{d}k}. \tag{A16}$$

The other arises from SLC,

$$\begin{aligned} \langle \kappa_\theta^3 \rangle^{\rm slc} &= 3 \langle \kappa_\theta^{(1)2} \kappa_\theta^{\rm slc(2)} \rangle \\ &= 9 \Omega_{\rm m} \left(\frac{H_0}{c}\right)^3 \int_0^{\chi_H} \mathrm{d}\chi n_{\rm s}(\chi) b(\chi) w(\chi) I_0(\chi) \\ &\quad \times \int_0^{\chi} \mathrm{d}\chi' g(\chi', \chi) w(\chi') I_0(\chi') - 6 V_\kappa(\theta) \\ &\quad \times \frac{H_0}{c} \int_0^{\chi_H} \mathrm{d}\chi n_{\rm s}(\chi) b(\chi) w(\chi) I_0(\chi). \end{aligned} \tag{A17}$$

To derive the last expression, we used an approximation, which turns out to be very accurate for top-hat smoothing (see B98 for details),

$$\frac{1}{2\pi} \int_0^{2\pi} \mathrm{d}\vartheta \sin\vartheta W(|\boldsymbol{k} + \boldsymbol{k}'|) \simeq W(k) W(k'), \tag{A18}$$

where ϑ is the angle between the wave vectors $\boldsymbol{k}$ and $\boldsymbol{k}'$, and $k = |\boldsymbol{k}|$.

Then, the convergence skewness simply reads, in the second-order perturbation theory framework, $S_3(\theta) = S_3^{\rm q.l.} + S_3^{\rm slc} = \langle \kappa_\theta^3 \rangle^{\rm q.l.} / V_\kappa^2(\theta) + \langle \kappa_\theta^3 \rangle^{\rm slc} / V_\kappa^2(\theta)$, where all the terms are computed above.

Note that our calculation is slightly different from that of B98. Indeed, B98 assumed an optimally weighted estimator for the convergence leading to equation (9) of his paper instead of our equation (A6). However, with approximation (A18), both estimators give the same results: equation (A11) would match equation (22) of B98, and therefore we would easily recover equation (29) of B98 for a scale-free power-spectrum.[4]

APPENDIX B: A BRIEF DESCRIPTION OF THE RAY-TRACING SIMULATIONS

In this Appendix, we describe the *N*-body data sets and the ray-tracing method used for this work. More technical details are presented by Hamana & Mellier (2001).

[4] Notice the difference of sign convention that we use for κ, to enforce positively for the convergence skewness.

Light-ray trajectories are followed through a large *N*-body simulation data set generated with a fully vectorized and parallelized particle–mesh (PM) code. Each *N*-body experiment involves $256^2 \times 512$ particles in a periodic rectangular box of size $(L,L,2L)$. The mesh used to compute the forces is $256^2 \times 512$. A light-cone of the particles is extracted from each simulation during the run as explained by Hamana, Colombi & Suto (2001). Our aim is for the light-cone to cover a large redshift range, $0 \leq z \lesssim 3$, and a field of view of $5^\circ \times 5^\circ$ square degrees. To do that, we adopt the tiling technique first proposed by White & Hu (2000): we perform 11 independent simulations covering adjacent redshift intervals $[z_i^{\rm min}, z_i^{\rm max}]$, $i = 1, \ldots, 11$. The size of each simulation is such that the portion of the light-cone in $[z_i^{\rm min}, z_i^{\rm max}]$ (aligned with the third axis) exactly fits the box-size. In this way, angular resolution is approximately conserved as a function of redshift, except close to the observer. Finally, in order to have enough structures in each box, we impose the supplementary constraint $L \geq 80 h^{-1}$ Mpc. As a result, L has the following sequence of values with redshift, 80, 80, 80, 80, 80, 120, 160, 240, 320, 480, $640\,h^{-1}$ Mpc.

The multiple lens-plane algorithm is used for ray-tracing calculations (Jain et al. 2000, and references therein). The lens planes (which are, at the same time, source planes) are separated by intervals of $80\,h^{-1}$ Mpc, amounting to a total number of 38 in the redshift range $0 \leq z \lesssim 3$. For each ray, the lensing magnification matrix is computed on the source planes and is stored. We perform 40 realizations of the underlying density field by random shifts of the simulation boxes in the (x,y) plane. For each realization, 512^2 rays are traced backward from the observer. The initial ray directions are set on 512^2 grids, which correspond to pixels of angular size $5^\circ/512 \sim 0.59$ arcmin.

Before using realistic redshift distribution of sources, we compute the skewness of the lensing convergence for single source planes, i.e. $n_{\rm s}(z) = \delta_{\rm D}(z = z_{\rm s})$ where $\delta_{\rm D}$ is the Dirac delta function. At this stage, we do not take into account the SLC effect. Fig. B1 shows S_3 obtained from the simulations compared with non-linear predictions. Measurements match theory reasonably well, as

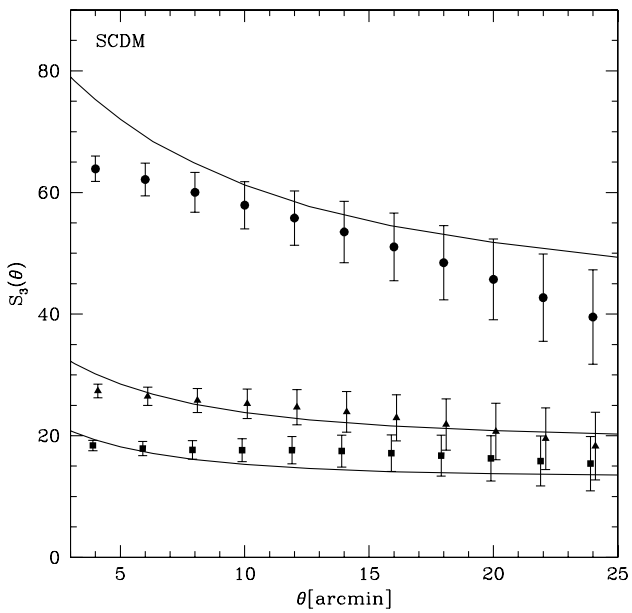

Figure B1. The skewness S_3 of the lensing convergence measured from the ray-tracing simulations (symbols) compared with non-linear predictions (solid lines) for single-source redshifts $z_{\rm s} \sim 1$ (top), 2 and 3 (bottom).

expected (Van Waerbeke et al. 2001b). There are slight differences, which can be explained as follows.

(i) The *N*-body simulations have a finite spatial resolution, which implies a flattening of S_3 at scales smaller than about 4 arcmin.

(ii) At large angular scales, $\theta \gtrsim 20-40$ arcmin, depending on the source redshift considered (Hamana & Mellier 2001), the measured S_3 underestimates the real value, owing to finite-volume effects [i.e. the lack of large-scale power, which contributes to the skewness on smaller scales, owing to the finite size of the simulation boxes (e.g. Colombi, Bouchet & Schaeffer 1994; see also Seto 1999).

(iii) There is an uncertainty in the fitting formula of the density bispectrum (Section 3), which transforms into a 10–20 per cent error on the semi-analytic prediction for S_3. The differences between theory and measurements in Fig. B1 are smaller than this expectation, at least in the range where the measurements are reliable, $4 \lesssim \theta \lesssim 20-40$ arcmin (derived from the above discussion on spatial resolution and finite-volume effects). It is important to note that this range is not equal to the dynamical range that the ray-tracing simulation originally has, which is much wider [see Hamana & Mellier (2001) for discussion on this point].

In conclusion, without SLC effects (yet) taken into account, the semi-analytic prediction obtained for S_3 is accurate (Van Waerbeke et al. 2001b).

APPENDIX C: PROCEDURE TO GENERATE MOCK GALAXY CATALOGUES

We have generated three mock galaxy catalogues with galaxy number counts $n_s(z)$ derived from the semi-analytic model by Devriendt & Guiderdoni (2000), and reproducing as well as possible the power-law model for the function $b(z)$, $b(z) = (1+z)^\gamma$ with $\gamma = 0$, 1, and 2. They are extracted from exactly the same dark matter distributions as used for the ray-tracing simulations.

The procedure to create the mock catalogues can be described as follows.

(i) We adopt threshold biasing, i.e. for a smooth density distribution of dark matter, we assume that galaxies lie in regions of density contrast larger than some threshold which may eventually depend on redshift [point (ii) below], $\delta \geq \delta_{\rm TH}(z)$. Inside these regions, the local number density of galaxies at position (z,θ,ϕ) [where z denotes the redshift and (θ,ϕ) denote the direction in the sky] is proportional to dark matter density,

$$n_{\rm g}(z,\theta,\phi) = \mu(z)[1+\delta(z,\theta,\phi)]. \quad \text{(C1)}$$

The normalization factor $\mu(z)$ is such that the redshift distribution of galaxies reproduces (in terms of an ensemble average) some prior, $n_s(z)$, discussed in (iii). To estimate the local density contrast from our discrete dark matter particle distribution, we use local adaptive smoothing: the mean quadratic distance d between each simulation particle and its six nearest neighbours is computed, $d^2 = \sum_{i=1}^{6} d_i^2$ where d_i is the separation between a central particle and the ith nearest neighbours. Then $1+\delta \propto d^{-3}$. For each dark matter particle in regions with $\delta > \delta_{\rm TH}$, N galaxies are randomly placed in the sphere of radius d centred on the particle position. N is computed from a random realization of a Poisson distribution with average $\bar{N} = (4/3)\pi d^3 n_{\rm g}$, where $n_{\rm g}$ is the mean number density of galaxies.

(ii) Function $\delta_{\rm TH}(z)$ is determined numerically so that the measured variances of density fluctuations in a sphere of radius $8\,h^{-1}$ Mpc in the galaxy and the dark matter distribution, respectively $\sigma_8^{\rm gal.}$ and σ_8, satisfy

$$\frac{\sigma_8^{\rm gal.}(z)}{\sigma_8(z)} = b(z). \quad \text{(C2)}$$

To do that, we use snapshots of the simulations at various redshifts z_i, and compute $\delta_{\rm TH}(z_i)$ iteratively to match equation (C2) within 3 per cent accuracy. Then function $\delta_{\rm TH}(z)$ is obtained by linear interpolation of $\delta_{\rm TH}(z_i)$. Note that since, for $\gamma = 0$, $b = 1$ irrespective of the redshift, the galaxy distribution directly traces the matter distribution, and thus we do not need to have a threshold, i.e. we simply set $\delta_{\rm TH} = \delta_{\rm min} - 1$.

(iii) A prior function $n_s(z)$ is needed to compute the normalization factor $\mu(z)$ (equation C1). We have used the *ab initio* semi-analytic approach to galaxy formation described by Devriendt & Guiderdoni (2000) to obtain a reasonably realistic estimate of this function. Such an approach is based on a Press–Schechter-like prescription to compute the number of galaxies as a function of redshift, coupled to spectrophotometric evolution of stellar populations to calculate their luminosities. The results naturally match observed galaxy number counts and redshift distributions, as well as the diffuse extragalactic background light for wavelengths ranging from the UV to the near IR. Here, we suppose that galaxies are selected in the *I* band, down to the magnitude $I_{AB} = 24.5$. As a result, the final mock catalogue yields a typical surface number density of 29 sources per arcmin^2 distributed in redshift as shown in Fig. C1. The distribution has a peak at $z \sim 0.4$, with mean redshift $\langle z \rangle \sim 0.8$ and typical width $\Delta z \sim 0.6$.

Note that, for $b > 1$, the linear bias prescription breaks down, because δ_s cannot be less than -1 by definition (in the perturbation theory approach, this does not cause a serious problem because $|\delta|$

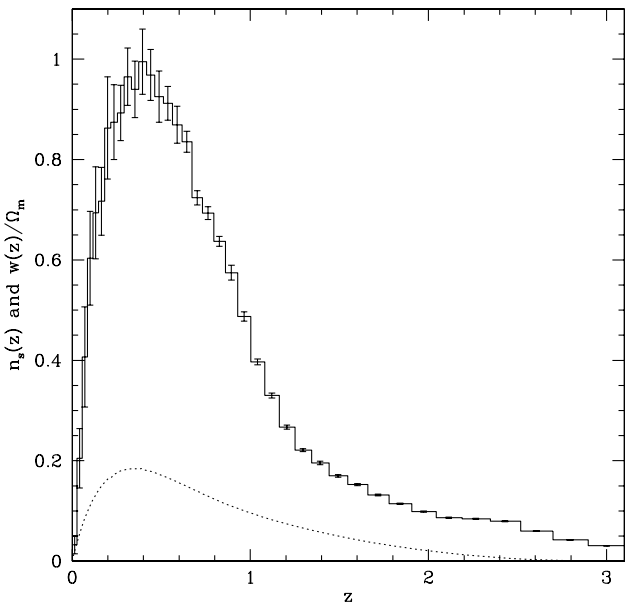

Figure C1. The distribution of sources (histogram with error bars) and the lensing efficiency function (dotted line) as functions of redshift. Error bars denote standard deviation computed among 40 realizations as discussed in Appendix B.

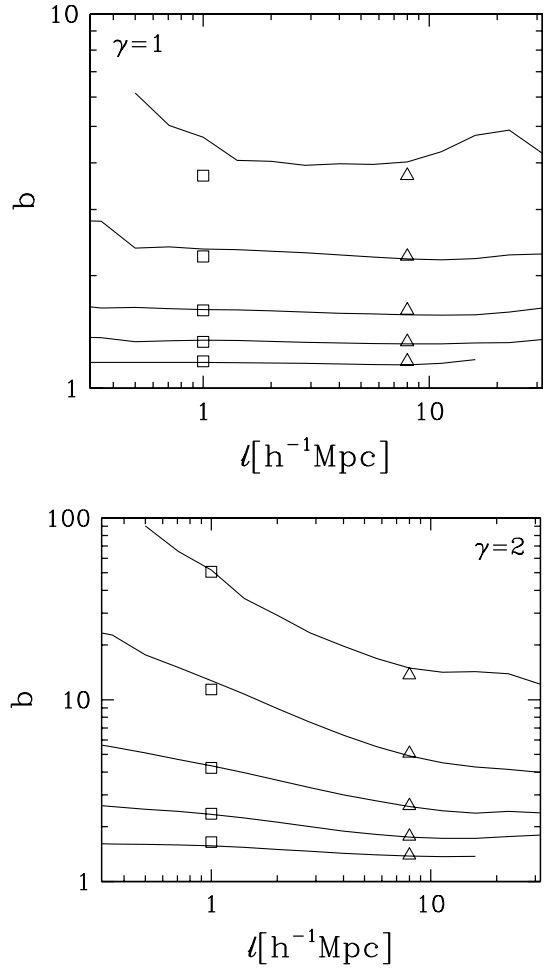

Figure C2. The biasing function $\tilde{b}$ [equation (C3)] as a function of spatial scale ℓ, measured in the mock galaxy catalogues. The top and bottom panels correspond respectively to $\gamma = 1$ and 2 (by construction, we have exactly $b = 1$ for $\gamma = 0$). Each curve is for a fixed value of z, namely $z \simeq 0.18$, 0.33, 0.62, 1.25 and 2.70 from bottom to top of each panel. In the top panel, the squares and the triangles give the values expected from $b(z) = 1 + z$. In the bottom panel, the squares and the triangles correspond respectively to $b(z) = (1 + z)^3$ and $b(z) = (1 + z)^2$.

is supposed to be much less than unity). Therefore we do not take the linear bias but use the threshold bias for the cases of $\gamma = 1$ and 2. Accordingly, strictly speaking, the direct comparison between the semi-analytical prediction and the numerical simulation makes sense only for the $\gamma = 0$ model. However, we take $\gamma = 1$ and 2 models to test the effect of the redshift evolution of bias which should not depend strongly on details of the biasing prescription. Moreover, to test the robustness of semi-analytic predictions in which the simple linear bias is used, it is interesting to use a different biasing prescription for the numerical experiments.

Fig. C2 shows the scaling behaviour of the bias factor defined by

$$\tilde{b}(z, \ell) \equiv \frac{\sigma_{\rm gal.}(\ell, z)}{\sigma(\ell, z)}, \tag{C3}$$

as measured in the mock catalogues with $\gamma = 1$ and 2. In this equation, $\sigma^2_{\rm gal.}(\ell)$ and $\sigma^2(\ell)$ are respectively the variances in a sphere of radius ℓ of the galaxy and the matter density distribution. In fact, we take for σ^2 the variance measured in the mock catalogue with $\gamma = 0$ which is unbiased by definition. To correct for variations of the selection function we use the method proposed by Colombi, Szapudi & Szalay (1998). The curves in each panel correspond to redshift slices of [0.16,0.20], [0.3,0.36], [0.56,0.68], [1.09,1.41] and [2.40,3.00].

By construction, the value of $\tilde{b}$ measured at $\ell = 8^{-1}$ Mpc (triangles) matches relation (C2) very well. However there is no guarantee for this result to hold at all scales. In other words, at fixed z, function $\tilde{b}(\ell,z)$ is not necessarily a constant of scale [and equal to $b(z) = (1 + z)^\gamma$], although this is pretty much the case for the $\gamma = 1$ mock catalogue.

For the $\gamma = 2$ mock catalogue, function $\tilde{b}(\ell,z)$ presents large variations with scale, increasing with redshift. This can be modelled as a varying effective $\tilde{\gamma}(\ell)$, for example $\tilde{\gamma} \simeq 3$ for $\ell = 1h^{-1}$ Mpc (squares in bottom panel of Fig. C2). While converting scales to angles, more relevant to our analysis, the modelling in terms of a function $\tilde{\gamma}(\theta)$ is not very convincing. Still, we find that in the range of interest, $4 \lesssim \theta \lesssim 20$–$30$ arcmin, we should compare measured SLC effects with semi-analytic predictions corresponding to $2 \lesssim \gamma \lesssim 3$.

This paper has been typeset from a TEX/LATEX file prepared by the author.